ALIEN EARTHS

Which Nearby Planetary Systems Are Likely to Host Habitable Planets and Life?

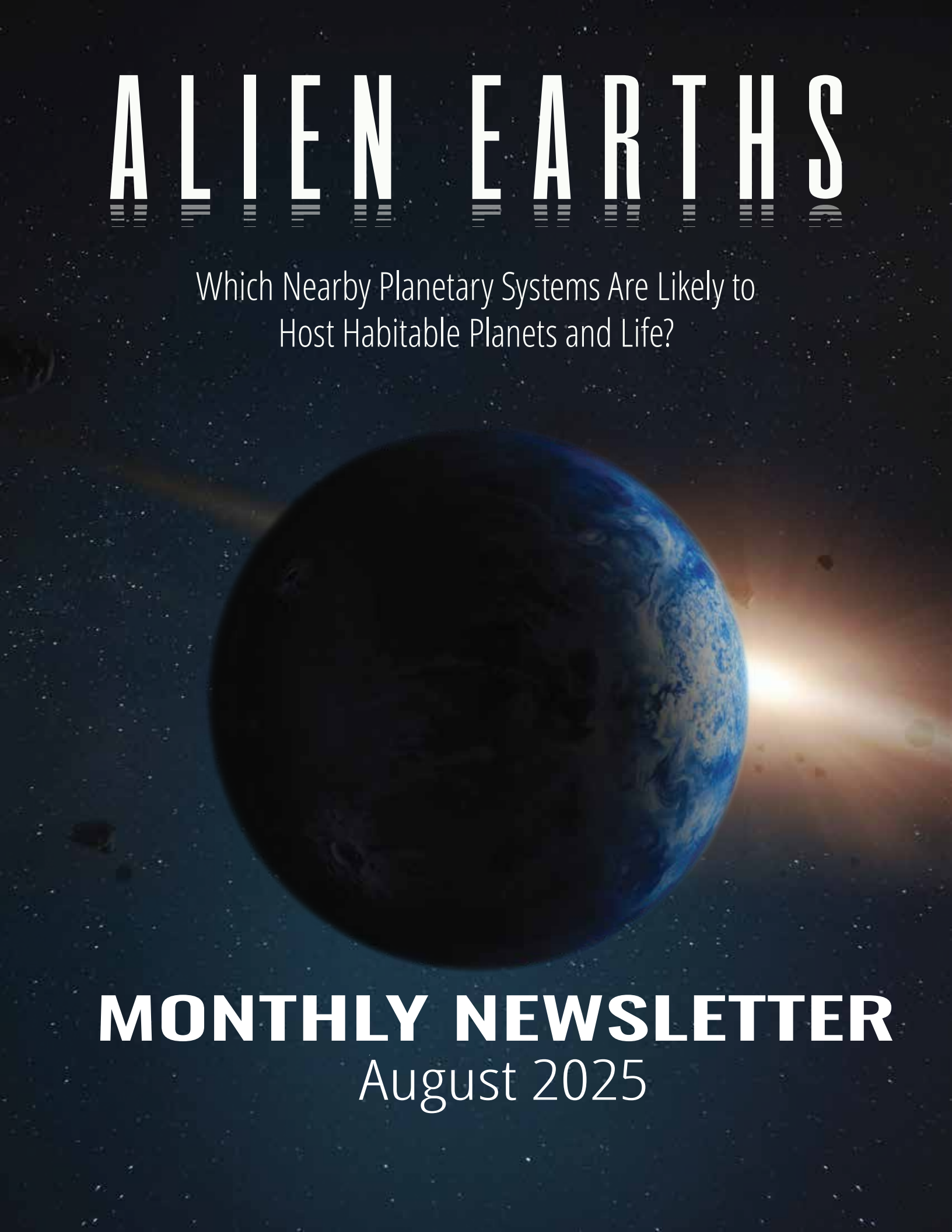

MONTHLY NEWSLETTER

August 2025

Message from the PI

Welcome to the August 2025 edition of the Alien Earths Newsletter! As we enter the final year of the Alien Earths project, I am impressed by all our team has achieved: Together with the precursor EOS project, Alien Earths now is in its 11th year and has led to over 250 refereed publications! Many of the EOS/AE papers had major impact on the field, receiving hundreds of citations and, in several cases, continue to shape the most important upcoming projects in exoplanet science and astrobiology. The two projects have supported about forty graduate students and postdoctoral researchers, and helped build interdisciplinary and international collaborations.

Over the past decade, we built a uniquely strong foundation and I am excited about what our team will accomplish in the coming year. A key challenge we faced was the lack of administrative support. I was happy to welcome Robin Stratton to Alien Earths. Robin joined us from Washington State University with extensive experience in research administration. Over the past two months, with her help, we were able to re-energize many of the AE activities that have slowed down over the past year. We updated the website, re-launched AE breakfasts, reviewing project progress and financial plans, and completed a postdoctoral search.

Although the funding landscape is shifting and the future is less predictable, I am confident that with the results, successes, and tools developed by our team position us well to extend our work to future opportunities. I look forward to the final year of Alien Earths and to continuing to work with you on advancing astrobiology and the search for life in the Universe.

Alien Earths on the Web

The Alien Earths website is currently undergoing renovations and will continue to be updated with new content. We are also building our presence on social media to share news, events, and program accomplishments. If you have news to share, please contact: rstratton@arizona.edu.

Alien Earths is part of NASA's Nexus for Exoplanetary System Science program, which carries out coordinated research toward the goal of searching for and determining the frequency of habitable extrasolar planets with atmospheric biosignatures in the Solar neighborhood.

Our interdisciplinary teams includes astrophysicists, planetary scientists, cosmochemists, material scientists, chemists, biologists, and physicists.

The Principal Investigator of Alien Earths is Daniel Apai (University of Arizona). The projects' lead institutions are The University of Arizona's Steward Observatory and Lunar and Planetary Laboratory.

For a complete list of publications, please visit the AE Library on the SAO/NASA Astrophysics Data System.

Welcome New Program Coordinator!

Robin Stratton joined the University of Arizona and Steward Observatory in May 2025 as the Research Program Administrator for Dr. Apai's group and Alien Earths. Bringing nearly three decades of experience as an administrative professional, she has extensive expertise in office operations, project coordination, financial management, and human resources and will be facilitating the administrative and financial support for the group.

Recent Publications

Signatures of Atmospheric Mass Loss and Planet Migration in the Time Evolution of Short-period Transiting Exoplanets

Bioverse: Potentially Observable Exoplanet Biosignature Patterns under the UV Threshold Hypothesis for the Origin of Life

A Terminology and Quantitative Framework for Assessing the Habitability of Solar System and Extraterrestrial Worlds

Orbital and Atmospheric Modeling of H II 1348B: An Eccentric Young Substellar Companion in the Pleiades

The CARMENES search for exoplanets around M dwarfs: Occurrence rates of Earth-like planets around very low-mass stars

TOI-6508 b: A massive transiting brown dwarf orbiting a low-mass star

Into the Mystic: the MUSE view of the ionized gas in the Mystic Mountains in Carina

The sensitivity to initial conditions of the co-orbital outcomes of lunar ejecta

Microstructural analysis of phosphorus (P)-bearing assemblages in type 3 chondrites: Implications for P condensation and processing in the early solar nebula

Bioverse: Giant Magellan Telescope and Extremely Large Telescope Direct Imaging and High-resolution Spectroscopy Assessment—Surveying Exo-Earth O_2 and Testing the Habitable Zone Oxygen Hypothesis

Interior Convection Regime, Host Star Luminosity, and Predicted Atmospheric CO2 Abundance in Terrestrial Exoplanets

Updated Spectral Characteristics for the Ultracool Dwarf TRAPPIST-1

HD 110067 c has an aligned orbit. Measuring the Rossiter-McLaughlin effect inside a resonant multi-planet system with ESPRESSO

Three short-period Earth-sized planets around M dwarfs discovered by TESS: TOI-5720 b, TOI-6008 b, and TOI-6086 b

Gliese 12 b: A Temperate Earth-sized Planet at 12 pc Ideal for Atmospheric Transmission Spectroscopy

Constraining Free–Free Emission and Photoevaporative Mass-loss Rates for Known Proplyds and New VLA–identified Candidate Proplyds in NGC 1977

Differences between Stable and Unstable Architectures of Compact Planetary Systems

August 2025 Newsletter Library

Signatures of Atmospheric Mass Loss and Planet Migration in the Time Evolution of Short-period Transiting Exoplanets

Fernandes, Rachel B.; Bergsten, Galen J.; Mulders, Gijs D.; Pascucci, Ilaria; Hardegree-Ullman, Kevin K.; Giacalone, Steven; Christiansen, Jessie L.; Rogers, James G.; Gupta, Akash; Dawson, Rebekah I.; Koskinen, Tommi T.; Boley, Kiersten M.; Curtis, Jason L.; Cunha, Katia; Mamajek, Eric E.; Sagynbayeva, Sabina; Bhure, Sakhee S.; Ciardi, David R.; Karpoor, Preethi R.; Pearson, Kyle A.; Zink, Jon K.; Feiden, Gregory A.

The Astronomical Journal, Volume 169, Issue 4

Comparative studies of young and old exoplanet populations offer a glimpse into how planets may form and evolve with time. We present an occurrence rate study of short-period (<12 days) planets between 1.8 and 10 $R_\oplus$ around 1374 FGK stars in nearby (200 pc) young clusters (<1 Gyr), utilizing data from the Transiting Exoplanet Survey Satellite mission. These planets represent a population closer to their primordial state. We find that the occurrence rate of young planets is higher (64−22+32%) compared to the Gyr-old population observed by Kepler (7.98−0.35+0.37%). Dividing our sample into bins of young (10–100 Myr) and intermediate (100 Myr–1 Gyr) ages, we also find that the occurrence distribution in orbital period remains unchanged, while the distribution in planet radius changes with time. Specifically, the radius distribution steepens with age, indicative of a larger planet population shrinking due to the atmospheric thermal cooling and mass loss. We also find evidence for an increase (1.9σ) in occurrence after 100 Myr, possibly due to tidal migration driving planets inside of 12 days. While evidence suggests that postdisk migration and atmospheric mass loss shape the population of short-period planets, more detections of young planets are needed to improve statistical comparisons with older planets. Detecting long-period young planets and planets <1.8 $R_\oplus$ will help us understand these processes better. Additionally, studying young planetary atmospheres provides insights into planet formation and the efficiency of atmospheric mass-loss mechanisms on the evolution of planetary systems.

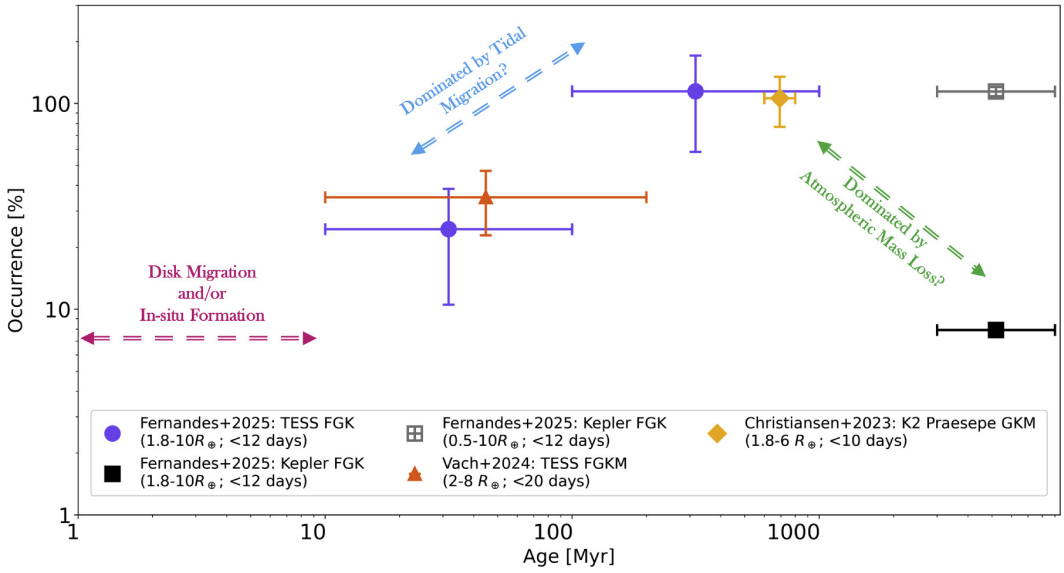

Figure 7. *Comparison of occurrence rates for sub-Neptunes and Neptunes from different surveys, with the various underlying mechanisms and their timelines depicted with dashed arrows.*

Bioverse: Potentially Observable Exoplanet Biosignature Patterns under the UV Threshold Hypothesis for the Origin of Life

Schlecker, Martin; Apai, Dániel; Affholder, Antonin; Ranjan, Sukrit; Ferrière, Régis; Hardegree-Ullman, Kevin K.; Lichtenberg, Tim; Mazevet, Stéphane

The Astrophysical Journal, Volume 987, Issue 1, id.24, 19 pp.

A wide variety of scenarios for the origin of life have been proposed, with many influencing the prevalence and distribution of biosignatures across exoplanet populations. This relationship suggests these scenarios can be tested by predicting biosignature distributions and comparing them with empirical data. Here, we demonstrate this approach by focusing on the cyanosulfidic origins-of-life scenario and investigating the hypothesis that a minimum near-ultraviolet (NUV) flux is necessary for abiogenesis. Using Bayesian modeling and the Bioverse survey simulator, we constrain the probability of obtaining strong evidence for or against this "UV Threshold Hypothesis" with future biosignature surveys. Our results indicate that a correlation between past NUV flux and current biosignature occurrence is testable for sample sizes of ≳50 planets. The diagnostic power of such tests is critically sensitive to the intrinsic abiogenesis rate and host star properties, particularly maximum past NUV fluxes. Surveys targeting a wide range of fluxes, and planets orbiting M dwarfs enhance the chances of conclusive results, with sample sizes ≳100 providing ≳80% likelihood of strong evidence if abiogenesis rates are high and the required NUV fluxes are moderate. For required fluxes exceeding a few hundred erg s−1 cm−2, both the fraction of inhabited planets and the diagnostic power sharply decrease. Our findings demonstrate the potential of exoplanet surveys to test origins-of-life hypotheses. Beyond specific scenarios, this work underscores the broader value of realistic survey simulations for future observatories (e.g., Habitable Worlds Observatory, LIFE, Extremely Large Telescopes, Nautilus) in identifying testable science questions, optimizing mission strategies, and advancing theoretical and experimental studies of abiogenesis.

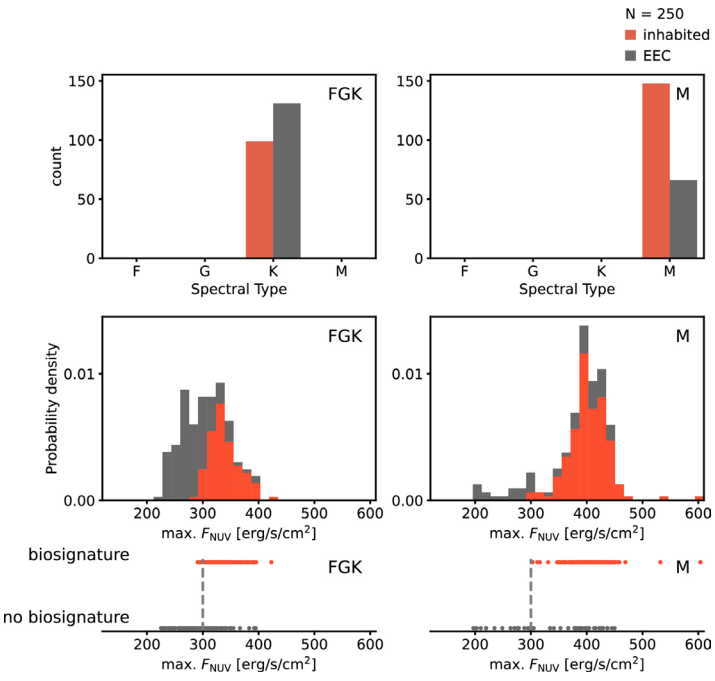

Figure 6. *Simulated transit surveys targeting FGK and M stars. Top panels: host stars of all transiting EECs and inhabited planets in a simulated transit survey. In the FGK sample, all EECs and all inhabited planets orbit K dwarfs. In an M dwarf sample of the same size, the fraction of inhabited planets is larger. Center panels: distribution of inferred maximum past NUV flux in transit surveys targeting EECs around FGK and M stars, respectively. The best-fit beta distributions correspond to selectivities of $s_{FGK} = -0.47$ and $s_M = -0.02$. Red areas show inhabited planets for an abiogenesis rate of $f_{life} = 0.8$ and a generic threshold NUV flux . Bottom panels: recovered biosignature detections and nondetections of simulated transit surveys. The dashed line denotes .*

A Terminology and Quantitative Framework for Assessing the Habitability of Solar System and Extraterrestrial Worlds

Apai, Dániel; Barnes, Rory; Murphy, Matthew M.; Lichtenberg, Tim; Tuchow, Noah; Ferrière, Régis; Wagner, Kevin; Affholder, Antonin; Malhotra, Renu; Journaux, Baptiste; Vazan, Allona; Ramirez, Ramses; Méndez, Abel; Kane, Stephen R.; Klawender, Veronica H. ; NExSS Quantitative Habitability Science Working Group

The Planetary Science Journal, Volume 6, Issue 7, id.165, 27 pp.

The search for extraterrestrial life in the solar system and beyond is a key science driver in astrobiology, planetary science, and astrophysics. A critical step is the identification and characterization of potential habitats, both to guide the search and to interpret its results. However, a well-accepted, self-consistent, flexible, and quantitative terminology and method of assessment of habitability are lacking. Our paper fills this gap based on a 3 yr long study by the NExSS Quantitative Habitability Science Working Group. We review past studies of habitability but find that the lack of a universally valid definition of life prohibits a universally applicable definition of habitability. A more nuanced approach is needed. We introduce a quantitative habitability assessment framework that enables self-consistent, probabilistic assessment of the compatibility of two models: first, a habitat model, which describes the probability distributions of key conditions in the habitat, and second, a viability model, which describes the probability that a metabolism is viable given a set of environmental conditions. We provide an open-source implementation of this framework and four examples as a proof of concept: (a) comparison of two exoplanets for observational target prioritization, (b) interpretation of atmospheric O_2 detection in two exoplanets, (c) subsurface habitability of Mars, and (d) ocean habitability in Europa. These examples demonstrate that our framework can self-consistently inform astrobiology research over a broad range of questions. The proposed framework is modular so that future work can expand the range and complexity of models available, both for habitats and for metabolisms.

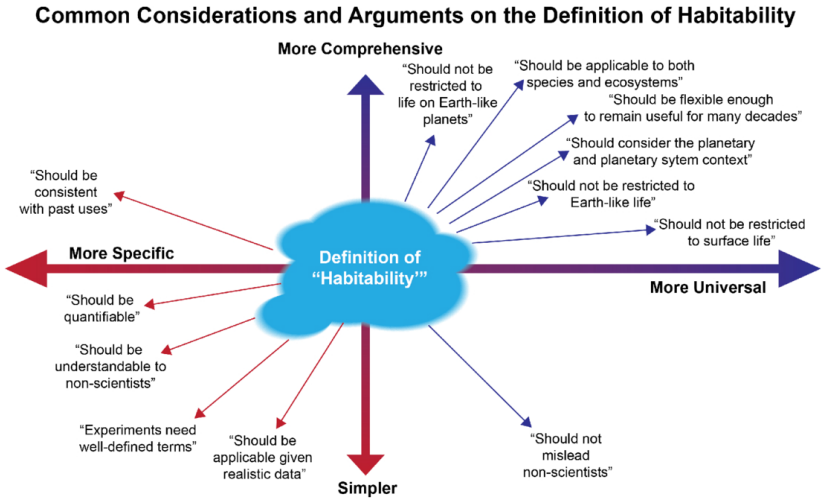

Figure 1. *Visual summary of key considerations and arguments about the nature and scope of the definition and use of the term "habitable." There are strong and valid arguments both for a simpler and more specific meaning and for a more complex and more universal meaning. Any single definition for "habitability" fails to meet the majority of the requirements.*

Orbital and Atmospheric Modeling of H II 1348B: An Eccentric Young Substellar Companion in the Pleiades

Weible, Gabriel; Wagner, Kevin; Stone, Jordan; Ertel, Steve; Apai, Dániel; Kratter, Kaitlin; Leisenring, Jarron

The Astronomical Journal, Volume 169, Issue 4, id.197, 21 pp.

Brown dwarfs with known physical properties (e.g., age and mass) are essential for constraining models of the formation and evolution of substellar objects. We present new high-contrast imaging observations of the circumbinary brown dwarf H II 1348B—one of the few known substellar companions in the Pleiades cluster. We observed the system in the infrared band with the Large Binocular Telescope Interferometer in dual-aperture direct-imaging mode (i.e., with the two telescope apertures used separately) on 2019 September 18. The observations attained a high signal-to-noise ratio (SNR > 150) photometric detection and relative astrometry with uncertainties of ∼5 mas. This work presents the first model of the companion's orbital motion using relative astrometry from five epochs across a total baseline of 23 yr. Orbital fits to the compiled data show the companion's semimajor axis to be with an eccentricity of . We infer that H II 1348B has a mass of 60–63 ± 2 M_J from comparison to brown dwarf evolutionary models given the well-constrained distance and age of the Pleiades. No other objects were detected in the H II 1348 system, and through synthetic planet injection and retrievals we establish detection limits at a cluster age of 112 ± 5 Myr down to ∼10–30 M_J for companions with projected separations of 21.5–280 au. With this work, H II 1348B becomes the second directly imaged substellar companion in the Pleiades with measured orbital motion after HD 23514B.

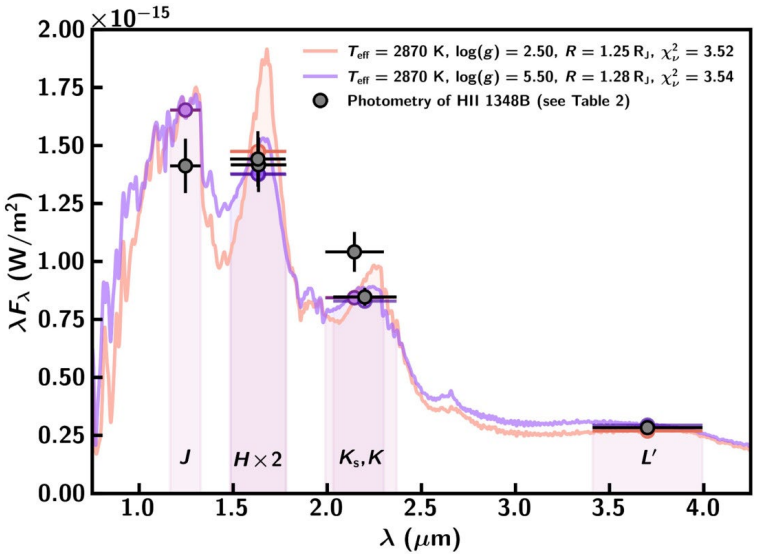

Figure 6. *Measured apparent photometry of H II 1348B from Table 2 is plotted in black with interpolated BT-SETTL (CIFIST 2011/2015) model spectra from MAP estimation plotted in salmon and purple. Synthetic photometry as integrated from the model spectra are shown in their respective colors with horizontal error bars spanning the shaded filter widths ($\Delta\lambda_{FWHM}$). Nonphysical, very low, and very high log(g) at grid edges are yielded by MAP estimation of the two posterior modes. The multiwavelength photometry of H II 1348 is inferred to be generally consistent with a late M spectral type, with no constraint on log(g). The interpolated model spectra are smoothed with a Gaussian filter to an average spectral resolution of R = 250 for the displayed wavelengths. Reduced chi-square values (χ_ν) are computed for 3 degrees of freedom: T_{eff}, log(g), and R.*

The CARMENES search for exoplanets around M dwarfs: Occurrence rates of Earth-like planets around very low-mass stars

Kaminski, A.; Sabotta, S.; Kemmer, J.; Chaturvedi, P.; Burn, R.; Morales, J. C.; Caballero, J. A.; Ribas, I.; Reiners, A.; Quirrenbach, A.; Amado, P. J.; Béjar, V. J. S.; Dreizler, S.; Guenther, E. W.; Hatzes, A. P.; Henning, Th.; Kürster, M.; Montes, D.; Nagel, E.; Pallé, E.; Pinter, V.; Reffert, S.; Schlecker, M.; Shan, Y.; Trifonov, T.; Osorio, M. R. Zapatero; Zechmeister, M.

Astronomy & Astrophysics, Volume 696, id.A101, 25 pp.

Aims. Previous estimates of planet occurrence rates in the CARMENES survey indicated increased numbers of planets on short orbits for M dwarfs with masses below 0.34$M_\odot$. Here we focused on the lowest-mass stars in the survey, comprising 15 inactive targets with masses under 0.16 $M_\odot$. Methods. To correct for detection biases, we determined detection sensitivity maps for individual targets and the entire sample. Using Monte Carlo simulations, we estimated planet occurrence rates for orbital periods of 1 d to 100 d and minimum masses from 0.5 $M_\oplus$ to 10$M_\oplus$. We also compared the actual sample of known planets to model predictions. Results. The radial velocity (RV) data from CARMENES reveal four new planets around three stars in our sample, namely G 268– 110 b, G 261–6 b, and G 192–15 b and c. All three b planets have minimum masses of 1.03–1.52 $M_\oplus$ and orbital periods of 1.43–5.45 d, while G 192–15 c is a 14.3 $M_\oplus$ planet on a wide, eccentric orbit with P ≈ 1218 d and e ≈ 0.68. Our occurrence rates suggest considerable dependencies with respect to stellar masses. For planets below 3 $M_\oplus$ we found rates consistent with one planet per star across all investigated periods, but the rates decrease almost by an order of magnitude for larger planet masses up to 10 $M_\oplus$. Compared to previous studies, low-mass stars tend to harbor more planets with P < 10 d. We also demonstrate that synthetic planet populations based on the standard core accretion scenario predict slightly more massive planets on wider orbits than observed. Conclusions. Our findings confirm that planet occurrence rates vary with stellar masses even among M dwarfs, as we found more planets with lower masses and on shorter orbits in our subsample of very low-mass stars compared to more massive M dwarfs. Therefore, we emphasize the need for additional differentiation in future studies.

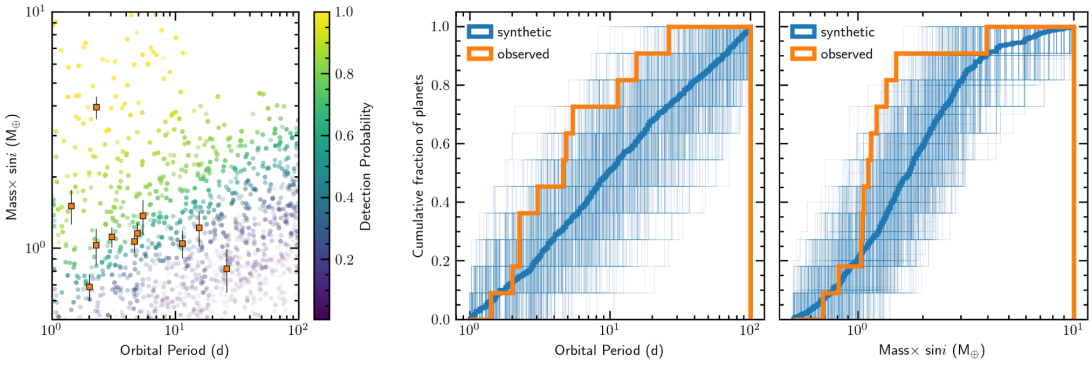

Figure 12. *Planet detection statistics of observed planets compared with mock detections based on the synthetic planet population by Burn et al. (2021). Included are all planets with orbital periods of 1–100 d and with minimum masses of 0.5–10 $M_\oplus$. The left panel shows the M_{pl} sin i of the observed (orange squares) and synthetic (circles) planets against orbital periods. The transparency and color of the synthetic data are scaled by detection probability. The cumulative distribution of the observed and synthetic P_{pl} (middle) and M_{pl} sin i (right) is shown. For the synthetic data, we show with transparent lines 1000 random draws of 11 planets to visualize the expected spread.*

TOI-6508 b: A massive transiting brown dwarf orbiting a low-mass star

Barkaoui, K.; Sebastian, D.; Zúñiga-Fernández, S.; Triaud, A. H. M. J.; Rackham, B. V.; Burgasser, A. J.; Carmichael, T. W.; Gillon, M.; Theissen, C.; Softich, E. ; Rojas-Ayala, B.; Srdoc, G. ; Soubkiou, A.; Fukui, A.; Timmermans, M. ; Stalport, M. ; Burdanov, A.; Ciardi, D. R. ; Collins, K. A. ; Davis, Y. T.; Davoudi, F.; de Wit, J.; Demory, B. O. ; Deveny, S.; Dransfield, G. ; Ducrot, E. ; Florian, L. ; Gan, T. ; Gómez Maqueo Chew, Y.; Hooton, M. J.; Howell, S. B.; Jenkins, J. M.; Littlefield, C.; Martín, E. L.; Murgas, F.; Niraula, P. ; Palle, E.; Pedersen, P. P. ; Pozuelos, F. J.; Queloz, D. ; Ricker, G. ; Schwarz, R. P. ; Seager, S.; Shporer, A. ; Scott, M. G.; Stockdale, C.; Winn, J.

Astronomy & Astrophysics, Volume 696, id.A44, 15 pp.

We report the discovery of a transiting brown dwarf orbiting a low-mass star, TOI-6508 b. Today, only ~50 transiting brown dwarfs have been discovered. TOI-6508 b was first detected with data from the Transiting Exoplanet Survey Satellite (TESS) in Sectors 10, 37 and 63. Ground-based follow-up photometric data were collected with the SPECULOOS-South (Search for habitable Planets EClipsing ULtra-cOOl Stars) and LCOGT-1m telescopes, and RV measurements were obtained with the Near InfraRed Planet Searcher (NIRPS) spectrograph. We find that TOI-6508 b has a mass of $M_p = 72.5_{-5.1}^{+7.6}$ M_{Jup} and a radius of $R_p = 1.03 \pm 0.03$ R_{Jup}. Our modeling shows that the data are consistent with an eccentric orbit of 19 day and an eccentricity of $e = 0.28_{-0.08}^{+0.09}$. TOI-6508 b has a mass ratio of $M_{BD}/M_\star = 0.40$, makes it the second highest mass ratio brown dwarf that transits a low-mass star. The host has a mass of $M_\star = 0.174 \pm 0.004$ $M_\odot$, a radius of $R_\star = 0.205 \pm 0.006$ $R_\odot$, an effective temperature of $T_{eff} = 2930 \pm 70$ K, and a metallicity of [Fe/H] = -0.22 ± 0.08. This makes TOI-6508 b an interesting discovery that has come to light in a region still sparsely populated.

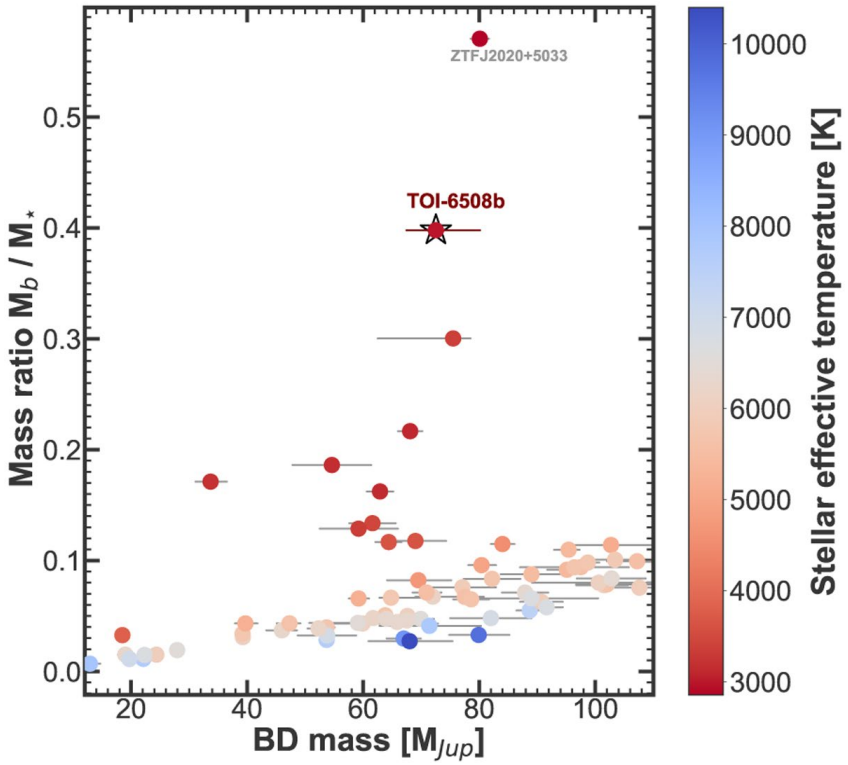

Figure 14. *Comparison of TOI-6508 b to other transiting BD systems from Table A.1. TOI-6508 b has the second highest mass ratio transiting BD after ZTF J2020+5033 (El-Badry et al. 2023). Dots are colored according to the stellar effective temperature.*

Into the Mystic: the MUSE view of the ionized gas in the Mystic Mountains in Carina

Reiter, Megan; McLeod, Anna F.; Itrich, Dominika; Klaassen, Pamela D.

Monthly Notices of the Royal Astronomical Society, Volume 537, Issue 4, pp.3009-3026

We present optical integral field unit observations of the Mystic Mountains, a dust pillar complex in the centre of the Carina Nebula that is heavily irradiated by the nearby young massive cluster Trumpler 14. With the continuous spatial and spectral coverage of data from the Multi-Unit Spectroscopic Explorer (MUSE), we measure the physical properties in the ionized gas including the electron density and temperature, excitation, and ionization. MUSE also provides an excellent view of the famous jets HH 901, 902, and 1066, revealing them to be high-density, low-ionization outflows despite the harsh environment. HH 901 shows spatially extended [C I] emission tracing the rapid dissociation of the photoevaporating molecular outflow in this highly irradiated source. We compute the photoevaporation rate of the Mystic Mountains and combine it with recent Atacama Large Millimeter Array observations of the cold molecular gas to estimate the remaining lifetime of the Mystic Mountains and the corresponding shielding time for the embedded protostars. The longest remaining lifetimes are for the smallest structures, suggesting that they have been compressed by ionizing feedback. Our data do not suggest that star formation in the Mystic Mountains has been triggered but it does point to the role that ionization-driven compression may play in enhancing the shielding of embedded stars and discs. Planet formation models suggest that the shielding time is a strong determinant of the mass and orbital architecture of planets, making it important to quantify in high-mass regions like Carina that represent the type of environment where most stars form.

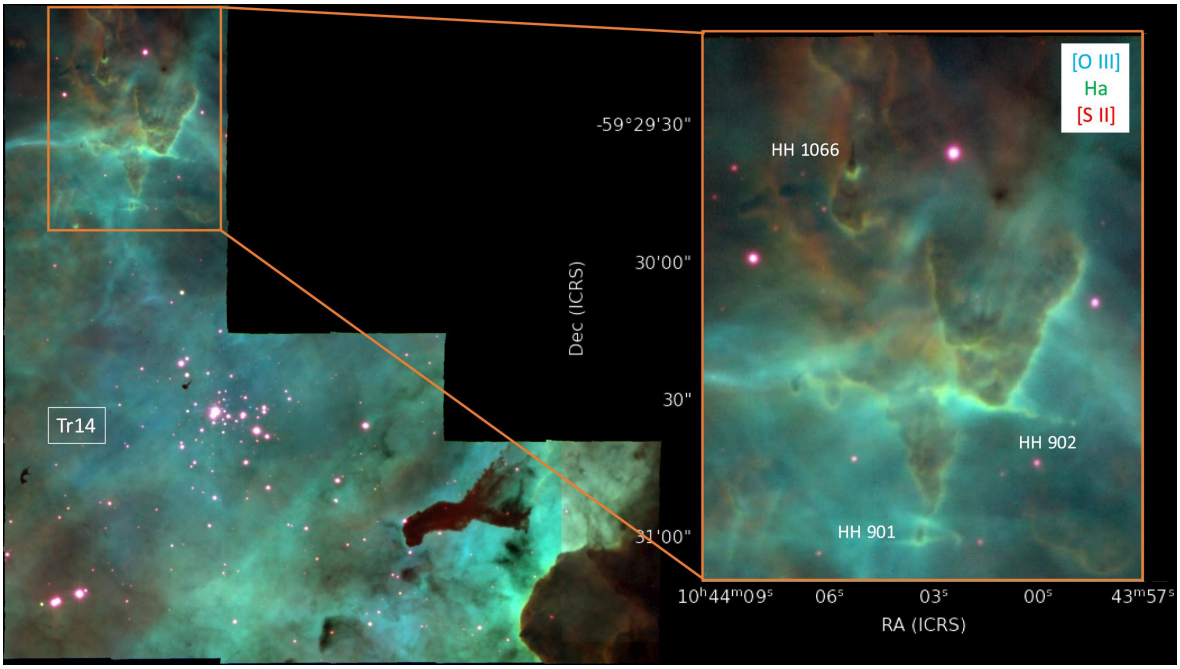

Figure 1. *Colour image showing the entire Tr14 MUSE survey area (north is up, east is to the left). The Mystic Mountains are pc to the north (in projection) of the Tr14 young massive cluster. The zoomed in image shown to the right highlights the subset of the data used in this work with the famous jets HH 901, HH 902, and HH 1066 labelled.*

The sensitivity to initial conditions of the co-orbital outcomes of lunar ejecta

Castro-Cisneros, Jose Daniel; Malhotra, Renu; Rosengren, Aaron J.

Icarus, Volume 429, id.116379

Lunar ejecta, produced by meteoroidal impacts, have been proposed for the origin of the near-Earth asteroid (469219) Kamo'oalewa, supported by its unusually Earth-like orbit and L-type reflectance spectrum (Sharkey et al., 2021). In a recent study (Castro-Cisneros et al. 2023), we found with N-body numerical simulations that the orbit of Kamo'oalewa is dynamically compatible with rare pathways of lunar ejecta captured into Earth's co-orbital region, persistently transitioning between horseshoe and quasi-satellite (HS-QS) states. Subsequently, Jiao et al. (2024) found with hydrodynamic and N-body simulations that the geologically young lunar crater Giordano Bruno generated up to 300 Kamo'oalewa-sized escaping fragments, and up to three of those could have become Earth co-orbitals. However, these results are based upon specific initial conditions of the major planets in the Solar System, close to the current epoch. In particular, over megayear time spans, Earth's eccentricity undergoes excursions up to five times its current value, potentially affecting the chaotic orbital evolution of lunar ejecta and their capture into Earth's co-orbital regions. In the present work, we carry out additional numerical simulations to compute the statistics of co-orbital outcomes across different launch epochs, representative of the full range of Earth's eccentricity values. Our main results are as follows: Kamo'oalewa-like co-orbital outcomes of lunar ejecta vary only slightly across the range of Earth's orbital eccentricity, suggesting no privileged ejecta launching epoch for such objects; the probability of co-orbital outcomes decreases rapidly with increasing launch speed, but long-lived HS-QS states are favored at higher launch speeds.

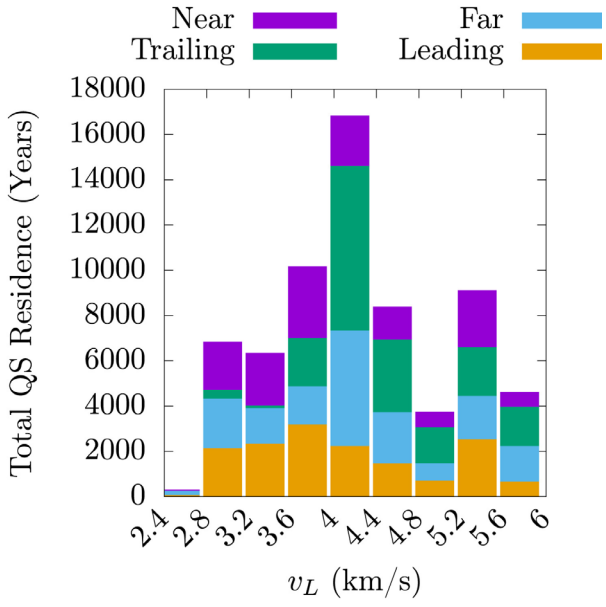

***Figure 10**. Total QS residence times as a function of the launch speed; the different colors indicate the contribution from each launch site. Longer QS residence times are favored for lunar ejecta launched from the trailing hemisphere at launch speeds near 4 km s^{-1}.*

Microstructural analysis of phosphorus (P)-bearing assemblages in type 3 chondrites: Implications for P condensation and processing in the early solar nebula

Benner, M. C. ; Manga, V. R. ; Prince, B. S. ; Ziurys, L. M. ; Zega, T. J.

Geochimica et Cosmochimica Acta, Volume 392, pp. 207-222

As the limiting element in the development of living systems, it is crucial to understand the history of phosphorus (P), from its stellar origins to its arrival on planetary surfaces. A key component in this cycle is understanding the forms of P delivered to the presolar nebula and their subsequent evolution on planetary bodies, including meteorites. Here, we report on the P distribution in the Bishunpur (LL3.15), Queen Alexandra Range (QUE) 97008 (L3.05), and Allan Hills (ALHA) 77307 (CO3.0) chondrites to determine its origins and secondary processing in the solar protoplanetary disk and on meteorite parent bodies using a coordinated analytical approach. In support of the microstructural characterization, we used density functional theory (DFT) to calculate the Gibbs free energy of the Fe_3P – Ni_3P binary under non-ideal mixing conditions in its entire range of composition and temperature space and performed equilibrium condensation modeling. We identified 106 P-bearing regions in these petrologic type-3 chondrites and find that the major P-bearing minerals are schreibersite ($(Fe, Ni)_3P$) and merrillite ($Ca_9NaMg(PO_4)_7$). Bishunpur predominately contains merrillite, which occurs in rims on chondrules and as hopper crystals. QUE 97008 primarily contains merrillite in association with metal and sulfides. Microstructural evaluation of merrillite in Bishunpur suggests igneous origins within the chondrule-forming region, whereas merrillite in QUE 97008 formed via condensation. In comparison, the dominant P-bearing phase in ALHA 77307 is P-bearing metal, including two Ni-rich schreibersite grains that are composed of 45 and 52.5 at.% Ni, far higher than predicted by equilibrium condensation. The equilibrium thermodynamic model, including our newly described non-ideal schreibersite solid solution, predicts the formation of a miscibility gap where $(Fe_{0.63}, Ni_{0.37})_3P$ and Ni_3P form via nebular condensation. We therefore suggest that Ni-rich schreibersite formed through non-equilibrium condensation.

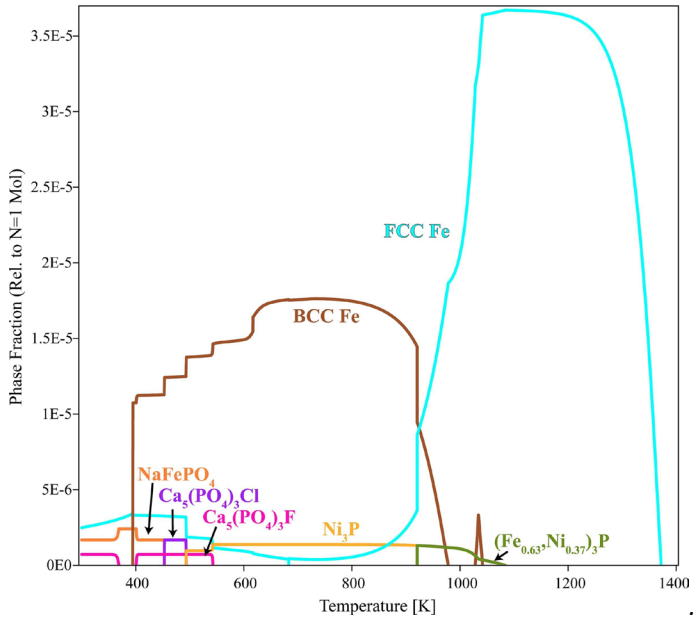

Figure 9. *Equilibrium condensation model of phosphates, metals, and schreibersite at $P = 10^{-4}$ bar with a cooling gas of solar composition. The abundances of elements are ratioed to a total system size of one mol (y-axis). The condensation sequence with schreibersite and metals in context can be found in supplementary Fig. 4.*

Bioverse: Giant Magellan Telescope and Extremely Large Telescope Direct Imaging and High-resolution Spectroscopy Assessment—Surveying Exo-Earth O2 and Testing the Habitable Zone Oxygen Hypothesis

Hardegree-Ullman, Kevin K.; Apai, Dániel; Haffert, Sebastiaan Y.; Schlecker, Martin; Kasper, Markus; Kammerer, Jens; Wagner, Kevin

The Astronomical Journal, Volume 169, Issue 3, id.171, 20 pp.

Biosignature detection in the atmospheres of Earth-like exoplanets is one of the most significant and ambitious goals for astronomy, astrobiology, and humanity. Molecular oxygen is among the strongest indicators of life on Earth, but it will be extremely difficult to detect via transmission spectroscopy. We used the Bioverse statistical framework to assess the ability to probe Earth-like O_2 levels on hypothetical nearby habitable zone exo-Earth candidates (EECs) using direct imaging and high-resolution spectroscopy on the Giant Magellan Telescope (GMT) and the Extremely Large Telescope (ELT). Assuming continued improvement in instruments and data processing, our analysis highlights the best-case scenarios. Earth-like O_2 levels could be probed on up to ∼7 and ∼19 EECs orbiting bright M dwarfs within 20 pc in a hypothetical 10 yr survey on the GMT and ELT, respectively. Four known super-Earth candidates, including Proxima Centauri b, could be probed for O_2 within about 1 week of observations on the ELT and a few months on the GMT. We also assessed the ability of the ELT to test the habitable zone oxygen hypothesis—that habitable zone Earth-sized planets are more likely to have O_2—within a 10 yr survey using Bioverse. Testing this hypothesis requires either ∼one-half of the EECs to have O_2 or ∼one-third if $\eta_\oplus$ is large. A Northern Hemisphere large-aperture telescope, such as the Thirty Meter Telescope, would expand the target star pool by about 25%, reduce the time to probe biosignatures on individual targets, and provide an additional independent check on potential biosignature detections.

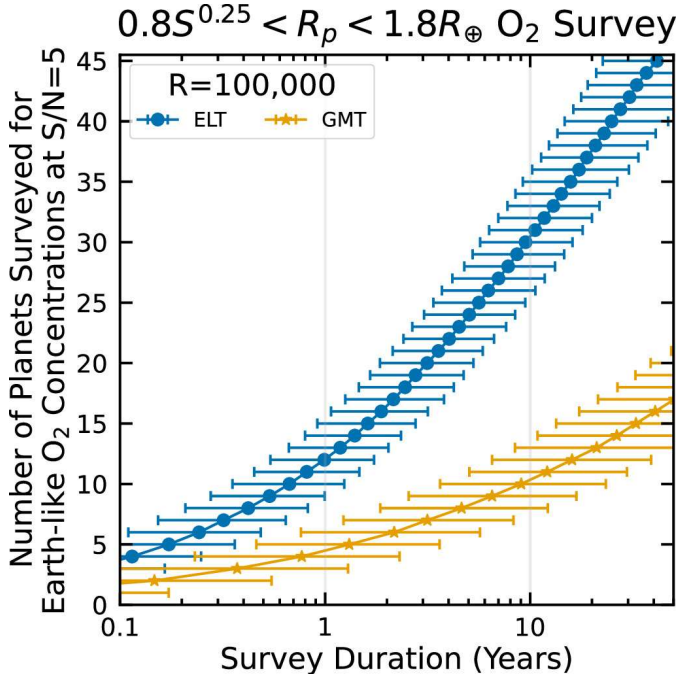

Figure 6. *Simulation results for a survey of Earth-like concentrations of O_2 at S/N = 5 on habitable zone Earth and super-Earth-sized candidates ($0.8S^{0.25} < R_p < 1.8\ R_\oplus$) within 20 pc with the ELT (blue dots) and the GMT (orange stars). Similar to the exo-Earth simulation in Figure 4, the ELT could probe about 3 times more planets than the GMT. Overall, a super-Earth survey could probe about 1.5 times more planets than a survey of planets up to 1.4 $R_\oplus$.*

Interior Convection Regime, Host Star Luminosity, and Predicted Atmospheric CO2 Abundance in Terrestrial Exoplanets

Affholder, Antonin; Mazevet, Stéphane; Sauterey, Boris; Apai, Dániel; Ferrière, Régis

The Astronomical Journal, Volume 169, Issue 3, id.125, 19 pp.

Terrestrial planets in the habitable zone (HZ) of Sun-like stars are priority targets for detection and observation by the next generation of space telescopes. Earth's long-term habitability may have been tied to the geological carbon cycle, a process critically facilitated by plate tectonics. In the modern Earth, plate motion corresponds to a mantle convection regime called mobile lid. The alternate, stagnant-lid regime is found on Mars and Venus, which may have lacked strong enough weathering feedback to sustain surface liquid water over geological timescales if initially present. Constraining observational strategies able to infer the most common regime in terrestrial exoplanets requires quantitative predictions of the atmospheric composition of planets in either regime. We use end-member models of volcanic outgassing and crust weathering for the stagnant- and mobile-lid convection regimes, which we couple to models of atmospheric chemistry and climate and ocean chemistry to simulate the atmospheric evolution of these worlds in the HZ. In our simulations under the two alternate regimes, we find that the fraction of planets possessing climates consistent with surface liquid water is virtually the same. Despite this unexpected similarity, we predict that a mission capable of detecting atmospheric CO_2 abundance above 0.1 bar in 25 terrestrial exoplanets is extremely likely (≥95% of samples) to infer the dominant interior convection regime in that sample with strong evidence (10:1 odds). This offers guidance for the specifications of the Habitable Worlds Observatory NASA concept mission and other future missions capable of probing samples of habitable exoplanets.

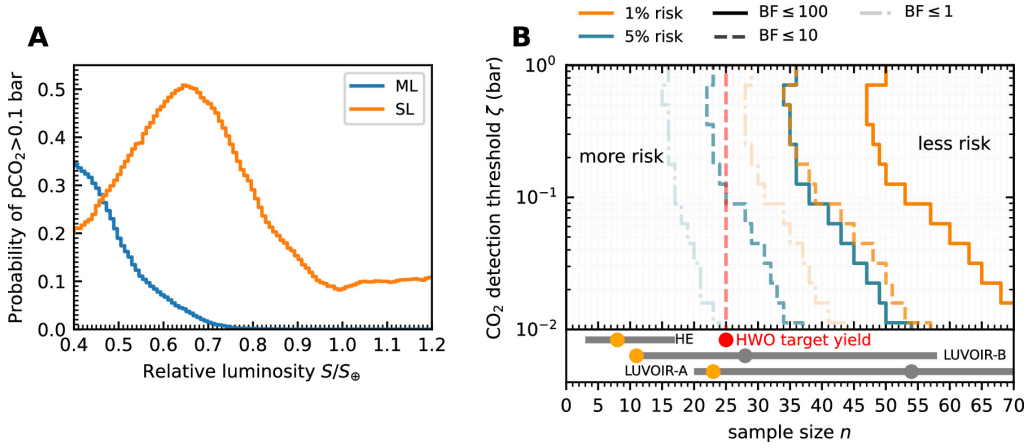

***Figure 7**. Probabilistic calculations for the inference of the dominant interior convection regime. (A) Estimate of the conditional probability P(Γ/S/S⊕) for each interior convection scenario used in Equation (38). (B) Inference risk (Equation (35)) over strategies of CO_2 detection threshold (ζ) and sample size (n). Orange (blue) lines indicate 1% (5%) risk contour levels. Solid lines map the risk that evidence in favor of the correct hypothesis is less than "extreme" (BF < 100). Dashed lines are the risk that evidence in favor of the correct hypothesis is less than "strong" (BF < 10). Semitransparent dashed and dotted lines are the risk that a sample yields stronger evidence in favor of the incorrect hypothesis than in favor of the correct one. The inset at the bottom shows the expected yield of different concepts of space observatories: LUVOIR (The LUVOIR Team 2019); HE, or HabEx (B. S. Gaudi et al. 2020); and HWO (E. Mamajek & K. Stapelfeldt 2024). The gray lines and circles indicate the expected number of EECs detected by each mission. Orange dots indicate the expected number of EEC spectra from each mission. The red dot indicates the target EEC spectra yield from the most recently proposed mission concept, HWO.*

Updated Spectral Characteristics for the Ultracool Dwarf TRAPPIST-1

Davoudi, Fatemeh; Rackham, Benjamin V.; Gillon, Michaël; de Wit, Julien; Burgasser, Adam J.; Delrez, Laetitia; Iyer, Aishwarya; Ducrot, Elsa

The Astrophysical Journal Letters, Volume 970, Issue 1, id.L4, 18 pp.

A comprehensive infrared spectroscopic study of star TRAPPIST-1 is a crucial step toward the detailed examination of its planets. While the presence of Earth's atmosphere has limited the spectral extent of such a study up to now, the Near Infrared Imager and Slitless Spectrograph (NIRISS) and the Near Infrared Spectrograph instruments aboard the James Webb Space Telescope (JWST) can now yield the 0.6–5 μm spectral energy distribution (SED) of the star. Here we translate TRAPPIST-1's SED into tight constraints on its luminosity (L_{bol} = 0.000566 ± 0.000022 $L_{\odot}$), effective temperature (T_{eff} = 2569 ± 28 K), and metallicity ([Fe/H] = 0.052 ± 0.073) and investigate the behavior of its gravity-sensitive indices. Through band-by-band comparisons of the NIRISS and ground-based spectra, TRAPPIST-1 exhibits a blend of both field source and intermediate-gravity spectral characteristics, suggesting that the star is likely a field-age source with spectral features reminiscent of young objects. We also employ photospheric modeling incorporating theoretical and JWST spectra to constrain stellar surface heterogeneities, finding that the limited fidelity of current stellar spectral models precludes definitive constraints on the physical parameters of the distinct spectral components giving rise to TRAPPIST-1's photospheric heterogeneity and variability. In addition, we find intermodel differences in the inferences of properties (e.g., the effective temperature) over one order of magnitude larger than the instrument-driven uncertainties (~100 K vs. ~4 K), pointing toward a model-driven accuracy wall. Our findings call for a new generation of stellar models to support the optimal mining of JWST data and further constraining stellar—and ultimately planetary—properties.

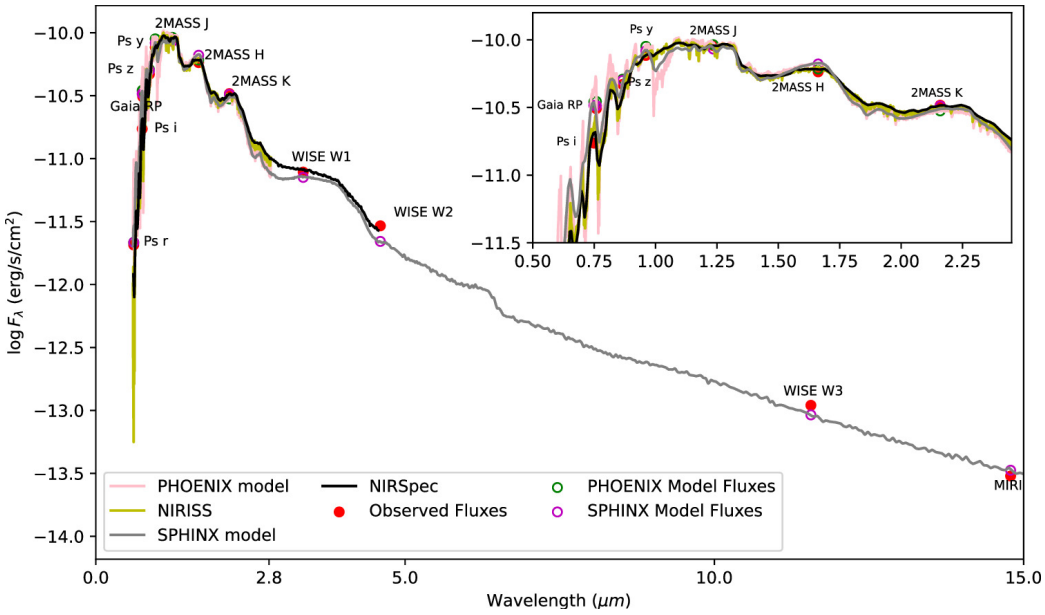

Figure 8*. Near-IR and IR SED of TRAPPIST-1. Red symbols represent the observed photometric measurements. Blue symbols are the model fluxes from the best-fit SPHNIX atmosphere model (gray). Overlaid on the model are the absolute flux-calibrated spectrophotometric observations from NIRISS (yellow) and NIRSpec (black).*

HD 110067 c has an aligned orbit. Measuring the Rossiter-McLaughlin effect inside a resonant multi-planet system with ESPRESSO

Zak, J.; Boffin, H. M. J.; Sedaghati, E.; Bocchieri, A.; Changeat, Q. ; Fukui, A. ; Hatzes, A.; Hillwig, T. ; Hornoch, K.; Itrich, D.; Ivanov, V. D.; Jones, D.; Kabath, P.; Kawai, Y. ; Mugnai, L. V.; Murgas, F.; Narita, N.; Palle, E. ; Pascale, E. ; Pravec, P. ; Redfield, S.; Roccetti, G.; Roth, M.; Srba, J. ; Tian, Q.; Tsiaras, A. ; Turrini, D.; Vignes, J. P.

Astronomy & Astrophysics, Volume 687, id.L2, 8 pp.

Planetary systems in mean motion resonances hold a special place among the planetary population. They allow us to study planet formation in great detail as dissipative processes are thought to have played an important role in their existence. Additionally, planetary masses in bright resonant systems can be independently measured via both radial velocities and transit timing variations. In principle, they also allow us to quickly determine the inclination of all planets in the system since, for the system to be stable, they are likely all in coplanar orbits. To describe the full dynamical state of the system, we also need the stellar obliquity, which provides the orbital alignment of a planet with respect to the spin of its host star and can be measured thanks to the Rossiter-McLaughlin effect. It was recently discovered that HD 110067 harbors a system of six sub-Neptunes in resonant chain orbits. We here analyze an ESPRESSO high-resolution spectroscopic time series of HD 110067 during the transit of planet c. We find the orbit of HD 110067 c to be well aligned, with a sky-projected obliquity of $\lambda = 6^{+24}_{-26}$ deg. This result indicates that the current architecture of the system was reached through convergent migration without any major disruptive events. Finally, we report transit-timing variation in this system as we find a significant offset of 19 ± 4 min in the center of the transit compared to the published ephemeris.

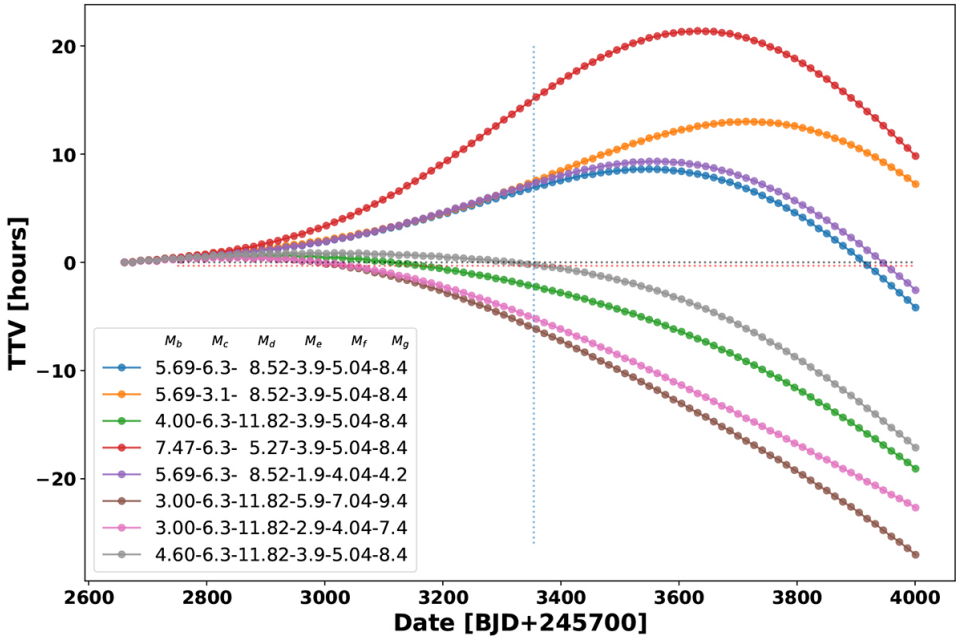

Figure 3. *Estimated TTVs for planet c in the system, for various planet masses, as indicated in the legend. The dashed vertical line marks the observing time with ESPRESSO. The dotted horizontal lines indicate no TTV (black) and a 19 min TTV (red).*

Three short-period Earth-sized planets around M dwarfs discovered by TESS: TOI-5720 b, TOI-6008 b, and TOI-6086 b

Barkaoui, K.; Schwarz, R. P.; Narita, N.; Mistry, P.; Magliano, C.; Hirano, T.; Maity, M.; Burgasser, A. J.; Rackham, B. V.; Murgas, F.; Pozuelos, F. J.; Stassun, K. G.; Everett, M. E.; Ciardi, D. R.; Lamman, C.; Pass, E. K.; Bieryla, A.; Aganze, C.; Esparza-Borges, E.; Collins, K. A.; Covone, G.; de Leon, J.; Dévora-Pajares, M.; de Wit, J.; Fukuda, Izuru; Fukui, A.; Gerasimov, R.; et al.

Astronomy & Astrophysics, Volume 687, id.A264, 24 pp.

One of the main goals of the NASA Transiting Exoplanet Survey Satellite (TESS) mission is the discovery of Earth-like planets around nearby M-dwarf stars. We present the discovery and validation of three new short-period Earth-sized planets orbiting nearby M dwarfs: TOI-5720 b, TOI-6008 b, and TOI-6086 b. We combined TESS data, ground-based multicolor light curves, ground-based optical and near-infrared spectroscopy, and Subaru/IRD radial velocity data to validate the planetary candidates and constrain the physical parameters of the systems. In addition, we used archival images, high-resolution imaging, and statistical validation techniques to support the planetary validation. TOI-5720 b is an Earth-sized planet with a radius of Rp = 1.09 $\pm$ 0.07 R$\oplus$. It orbits a nearby (36 pc) M 2.5 host with an orbital period of P = 1.4344555 $\pm$ 0.0000036 days. It has an equilibrium temperature of Teq = 708 $\pm$ 19 K (assuming a null albedo) and an incident flux of Sp = 41.7 $\pm$ 4.5 S$\oplus$. TOI-6008 b is a short-period planet of P = 0.8574347 $\pm$ 0.0000424 day. It has a radius of Rp = 1.03 $\pm$ 0.05 R$\oplus$, an equilibrium temperature of Teq = 707 $\pm$ 19 K, and an incident flux of Sp = 41.5 $\pm$ 4.5 S$\oplus$. The host star (TOI-6008) is a nearby (23 pc) M 5 with an effective temperature of Teff = 3075 $\pm$ 75 K. Based on the radial velocity measurements collected with Subaru/IRD, we set a 3 σ upper limit of Mp < 4 M$\oplus$, thus ruling out a star or brown dwarf as the transiting companion. TOI-6086 b orbits its nearby (32 pc) M 3 host star (Teff = 3200 $\pm$ 75 K) every 1.3888725 $\pm$ 0.0000827 days and has a radius of Rp = 1.18 $\pm$ 0.07 R$\oplus$, an equilibrium temperature of Teq = 634 $\pm$ 16 K, and an incident flux of Sp = 26.8 $\pm$ 2.7 S$\oplus$. Additional high-precision radial velocity measurements are needed to derive the planetary masses and bulk densities and to search for additional planets in the systems. Moreover, short-period Earth-sized planets orbiting around nearby M dwarfs are suitable targets for an atmospheric characterization with the James Webb Space Telescope through transmission and emission spectroscopy and phase-curve photometry.

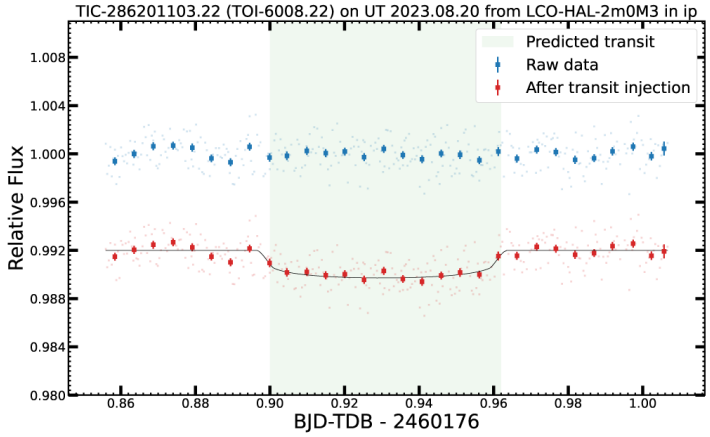

***Figure 11**. LCO-HAL-2 m0/MuSCAT photometry of TOI-6008.22 collected on UT August 20, 2023 in the Sloan-i' filter with an exposure time of 30s. The blue data points show the raw light curve. The red data points show the light curve after the transit injection of an Earth-sized planet of ~1.12 $R_\oplus$ with the best-fitting model superimposed in black. The green region shows the predicted ingress and egress of the transit. The light curves are shifted along the y-axis for clarity.*

Gliese 12 b: A Temperate Earth-sized Planet at 12 pc Ideal for Atmospheric Transmission Spectroscopy

Kuzuhara, Masayuki; Fukui, Akihiko; Livingston, John H.; Caballero, José A.; de Leon, Jerome P.; Hirano, Teruyuki; Kasagi, Yui; Murgas, Felipe; Narita, Norio; Omiya, Masashi; Orell-Miquel, Jaume; Palle, Enric; Changeat, Quentin; Esparza-Borges, Emma; Harakawa, Hiroki; Hellier, Coel; Hori, Yasunori; Ikuta, Kai; Ishikawa, Hiroyuki Tako; Kodama, Takanori; Kotani, Takayuki; et al.

The Astrophysical Journal Letters, Volume 967, Issue 2, id.L21, 24 pp.

Recent discoveries of Earth-sized planets transiting nearby M dwarfs have made it possible to characterize the atmospheres of terrestrial planets via follow-up spectroscopic observations. However, the number of such planets receiving low insolation is still small, limiting our ability to understand the diversity of the atmospheric composition and climates of temperate terrestrial planets. We report the discovery of an Earth-sized planet transiting the nearby (12 pc) inactive M3.0 dwarf Gliese 12 (TOI-6251) with an orbital period (P orb) of 12.76 days. The planet, Gliese 12 b, was initially identified as a candidate with an ambiguous P orb from TESS data. We confirmed the transit signal and P orb using ground-based photometry with MuSCAT2 and MuSCAT3, and validated the planetary nature of the signal using high-resolution images from Gemini/NIRI and Keck/NIRC2 as well as radial velocity (RV) measurements from the InfraRed Doppler instrument on the Subaru 8.2 m telescope and from CARMENES on the CAHA 3.5 m telescope. X-ray observations with XMM-Newton showed the host star is inactive, with an X-ray-to-bolometric luminosity ratio of . Joint analysis of the light curves and RV measurements revealed that Gliese 12 b has a radius of 0.96 $\pm$ 0.05 R $\oplus$, a 3 σ mass upper limit of 3.9 M $\oplus$, and an equilibrium temperature of 315 $\pm$ 6 K assuming zero albedo. The transmission spectroscopy metric (TSM) value of Gliese 12 b is close to the TSM values of the TRAPPIST-1 planets, adding Gliese 12 b to the small list of potentially terrestrial, temperate planets amenable to atmospheric characterization with JWST.

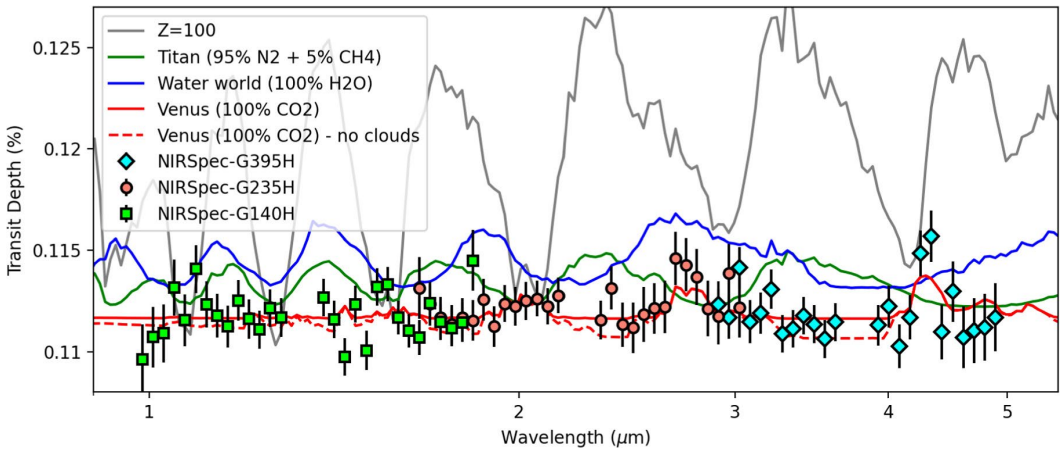

***Figure 10**. Predicted transmission spectra for Gliese 12 b, assuming an isothermal temperature–pressure profile, an Earth-like density, and several different cloud-free compositions: primordial H2 and He at 100× solar metallicity, Titan-like, water world, and Venus-like. For the Venus-like scenario, we also show a model including 0.1 bar fully opaque clouds. We show simulated data assuming the cloudy Venus scenario and six transits per JWST/NIRSpec grism: G140H (green squares), G235H (red circles), and G395H (blue diamonds).*

Constraining Free–Free Emission and Photoevaporative Mass-loss Rates for Known Proplyds and New VLA–identified Candidate Proplyds in NGC 1977

Boyden, Ryan D.; Eisner, Josh A.

The Astrophysical Journal, Volume 967, Issue 2, id.103, 23 pp.

We present NSF's Karl G. Jansky Very Large Array observations covering the NGC 1977 region at 3.0, 6.4, and 15.0 GHz. We search for compact radio sources and detect continuum emission from 34 NGC 1977 cluster members and 37 background objects. Of the 34 radio-detected cluster members, 3 are associated with known proplyds in NGC 1977, 22 are associated with additional young stellar objects in NGC 1977, and 9 are newly identified cluster members. We examine the radio spectral energy distributions, circular polarization, and variability of the detected NGC 1977 sources and identify 10 new candidate proplyds whose radio fluxes are dominated by optically thin free–free emission. We use measurements of free–free emission to calculate the mass-loss rates of known proplyds and new candidate proplyds in NGC 1977, and find values ~10-9 to 10-8 M ⊙ yr-1, which are lower than the mass-loss rates measured toward proplyds in the Orion Nebula Cluster but consistent with the mass-loss rates predicted by external photoevaporation models for spatially extended disks that are irradiated by the typical external ultraviolet (UV) fields encountered in NGC 1977. Finally, we show that photoevaporative disk winds in NGC 1977 may be illuminated by internal or external sources of ionization, depending on their positions within the cluster. This study provides new constraints on disk properties in a clustered star-forming region with a weaker UV environment than the Orion Nebula Cluster but a stronger UV environment than low-mass star-forming regions like Taurus. Such intermediate UV environments represent the typical conditions of Galactic star and planet formation.

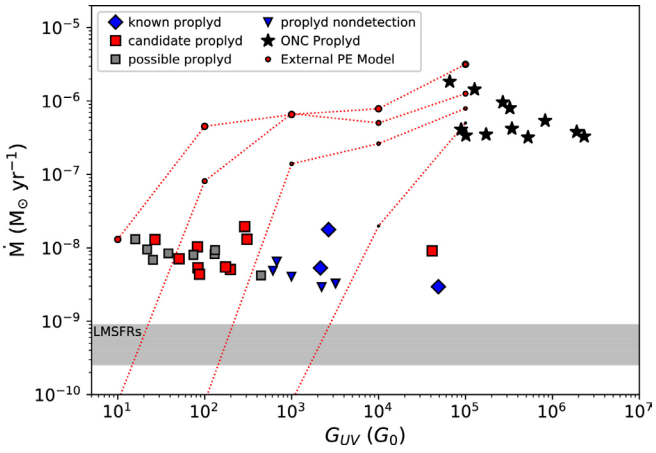

Figure 8. *Photoevaporative mass-loss rates ($\dot{M}$) derived from Equation (3) for all known, candidate, and possible NGC 1977 proplyds detected in our VLA maps, plotted as a function of the local FUV radiation field strength. We also include points showing the mass-loss rates inferred from the 4σ 6.4 GHz upper flux limits measured toward the VLA-nondetected known proplyds from Bally et al. (2012) and Kim et al. (2016). We also show the mass-loss rates derived by Ballering et al. (2023) for a subset of ALMA-detected proplyds in the ONC, where the FUV radiation field strength toward the ONC proplyds is calculated using an FUV photon luminosity of 7.0 × 10^{48} s^{-1} for ϑ^1 Ori C (Johnstone et al. 1998; Störzer & Hollenbach 1999; O'Dell et al. 2017), which we assume as the sole, dominant source of external FUV radiation in our calculations. The shaded gray region indicates the 1σ region around the median internally driven wind mass-loss rates derived by Fang et al. (2018) toward a sample of disks in low-mass star-forming regions. The dotted red lines show predicted mass-loss rates (as a function of the FUV field strength) from the FRIED grid of externally evaporating disk models (Haworth et al. 2018b), with the different lines corresponding to models with different disk radii. The model disk size is directly proportional to the size of the plotted red circles, and we show the predicted mass-loss rates for disk radii of 20, 40, 75, and 150 au (from smallest to largest circles). All plotted models share a common initial disk mass of ~5 Jupiter masses and a common central stellar mass of ~0.5 M ⊙.*

Differences between Stable and Unstable Architectures of Compact Planetary Systems

Volk, Kathryn; Malhotra, Renu

The Astronomical Journal, Volume 167, Issue 6, id.271, 14 pp.

We present a stability analysis of a large set of simulated planetary systems of three or more planets based on architectures of multiplanet systems discovered by Kepler and K2. We propagated 21,400 simulated planetary systems up to 5 billion orbits of the innermost planet; approximately 13% of these simulations ended in a planet–planet collision within that time span. We examined trends in dynamical stability based on dynamical spacings, orbital period ratios, and mass ratios of nearest-neighbor planets as well as the system-wide planet mass distribution and the spectral fraction describing the system's short-term evolution. We find that instability is more likely in planetary systems with adjacent planet pairs that have period ratios less than 2 and in systems of greater variance of planet masses. Systems with planet pairs at very small dynamical spacings (less than ~10–12 mutual Hill radii) are also prone to instabilities, but instabilities also occur at much larger planetary separations. We find that a large spectral fraction (calculated from short integrations) is a reasonable predictor of longer-term dynamical instability; systems that have a large number of Fourier components in their eccentricity vectors are prone to secular chaos and subsequent eccentricity growth and instabilities.

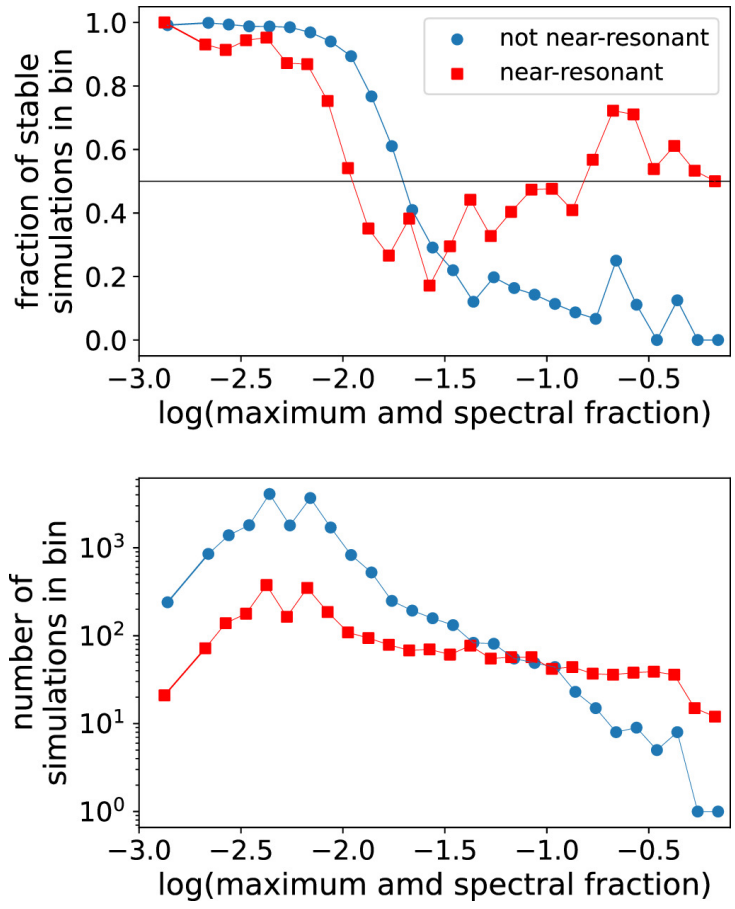

Figure 12. *All simulations: fraction of stable simulations as a function of the largest AMD spectral fraction for any planet in that simulation (top) and number of simulations per spectral fraction bin (bottom). Planetary systems without planet pairs starting obviously near strong MMRs (systems with MMRs labeled as 0 or 2 in Table 2) are shown as blue dots, while those that are likely in or near resonance are shown as red squares (systems with MMRs labeled as 1 in Table 2). These plots include all simulations performed (whether the planets masses were assigned from the mass–radius relationship or from TTV/RV measurements) that survived for at least 10^6 orbits, the minimum time span to perform a useful FFT.*